Chapter 5
Modeling Cascading Failures in Power Systems: Quasi-Steady-State Models and Dynamic Models

Eduardo Cotilla-Sanchez

Nomenclature

QSS	Quasi-Steady-State.
$p.u.$	per unit.
N	Number of buses in the system.
NM	Number of branches in the system (transmission lines and transformers).
N_G	The set of all generator buses in the system $N_G \subset n = \{1, 2, \ldots, N\}$.
N_D	The set of all demand/load buses in the system $N_D \subset n = \{1, 2, \ldots, N\}$.
MW	Megawatts.
C	Set of contingencies $C = \{c_1, c_2, \ldots\}$.
m_i	Cascading simulator model i .
R	Relative agreement of cascading path.
$r_{g,i}$	Generator equivalent series resistance.
$X_{d,i}$	Direct axis synchronous reactance for the generator at Bus i. $X'_{d,i}$ is the transient reactance. X_q refers to the quadrature axis reactance.
M	Generator inertia constant.
D	Generator damping constant.
$\tilde{V}_i$	Complex voltage at Bus i: $\tilde{V}_i = \lvert V_i \rvert e^{j\theta_i}$.

E. Cotilla-Sanchez (✉)
Kelley Engineering Center, Oregon State University, Corvallis, OR, USA
e-mail: ecs@oregonstate.edu

K. Sun (ed.), *Cascading Failures in Power Grids*, Power Electronics and Power Systems, https://doi.org/10.1007/978-3-031-48000-3_5

5.1 Modeling Cascading Failures in Power Systems: Quasi-Steady-State Models and Dynamic Models

5.1.1 Introduction

In essence, cascading failures emerge when outage mechanisms interact and show dependency patterns. Because modern grids incorporate new devices with new modes of becoming unstable, and these contribute to increasing the complexity of cascades, it becomes very important to understand how to place an upper bound on the modeling needs that one should implement when performing cascading analysis.

Generally for advanced simulation of cascading outages, it is understood that we need the ingredients of dynamics and protection. However, in a majority of current approaches to simulating cascading, the efforts to model dynamics and protection are either shorthanded or so detailed that results are difficult to interpret and benchmark [8]. The challenges on choosing appropriate timescales between quasi-steady-state and dynamic simulations, or other solutions, such as quasi-dynamic implementations, are also well justified in [14, 22]. An intended contribution of this chapter is to discuss and compare example simulators and experiments that have comparable protection elements and tunable dynamics in an open-source platform.

Recently, Dai et al. [5] show that security dispatches with multiple constraints can increase cascading outage risk due to overload of critical lines. They also compare a QSS simulator and a dynamic simulator for their experiments. Similarly, counter-intuitive relationships between system loading levels and cascading risk were observed by [19] using the QSS simulator that we compare in this work with a closely related dynamic simulator. This work shows that increased risk can be observed at lower demand levels.

One of the major challenges in the simulation is how to handle islands. This is necessary, and while some QSS simulators explicitly address separation and how to account for those (lines or load) losses, some of the dynamic simulators present challenges upon stability of islands. There are efforts to study the post-disturbance stability guarantees [16], and research groups have also explored control strategies to reconnect at appropriate times and mitigate further separation and damage [15].

Along with relatively recent benchmarking efforts, [2], the recommended standards to implement within these proposed benchmarks have also evolved and increasingly include additional types of relay mechanisms in cascading studies. Back to the PRC-023-2 standard, from 2012, one out of three mechanisms (overloads) could be implemented with a QSS simulator; however, the remainder of mechanisms requires some level of dynamic modeling. Newer standards and mechanisms, for example, inverter-interfaced renewable generation, will continue to push the complexity of required studies without a clear path to equitable compare across the methodologies used by different utilities, for example.

More recent benchmarking studies, e.g., [11] by the IEEE Cascading Failure Working Group, have broadly implemented analysis with multiple simulators, including research-grade (sometimes open source) and commercial-grade method-

ologies. The QSS simulation templates in [11] are used as baseline in this chapter for the proposed experiments in the remainder of this chapter.

5.1.2 Metrics to Benchmark Experiments with QSS and Dynamic Simulators

In addition to common cascade and resulting blackout statistics seen in previous benchmark studies, we adapt a metric of cascade path similarity, first introduced in [7] (Evaluating the Impact of Modeling Assumptions for Cascading Failure Simulation), the *Relative Agreement of Cascading Path*, R, defined as follows:

$$R(m_1, m_2) = \frac{1}{|C|} \sum_{i=1}^{|C|} \frac{|A_i \cap B_i|}{|A_i \cup B_i|}, \tag{5.1}$$

where m_1 and m_2 are the two cascading simulators being compared, A_i and B_i are the sets of dependent events for each cascade, and C is the set of cascades under consideration. In summary, for all experiments developed in this chapter, we measure and record the following statistics at the end of each cascade simulation, for each simulator:

- Blackout size: Total unserved load in per unit MW
- Cascade size: The number of line failures and their sequence
- Relative agreement of cascading path: R, defined as in Eq. 5.1

Similar to these, as well as other related metrics, are regularly used to assess risk derived from cascading outages or common mode failures [17, 18]. Real datasets derived from transmission owners are particularly valuable and help calibrate simulator models. In [17], the authors cluster and analyze data from the NERC TADS (Transmission Availability Data System), obtaining useful results about the timing of the outages. They also highlight the opportunity to use an underlying network model so that electrical distance for the clusters of outages can be included in the analysis.

5.1.3 A QSS Model Example

The quasi-steady-state (QSS) example model *dcsimsep* [12] is used here to investigate assumptions of models that rely solely on the steady-state operation of the system. There are no generator or load dynamics in the model, and the only departures from steady-state conditions come from relay-based switching of overloaded transmission lines.

The *dcsimsep* simulator was originally developed at the University of Vermont, led by Prof. Paul Hines and with contributions by Dr. Pooya Rezaei, Prof. Maggie Eppstein, as well as the author of this chapter. While the horizon timeline is simplified into QSS and the power flow implemented uses the dc approximation, the simulator features a relatively sophisticated separation (islanding) scheme and the possibility to interface with external solvers to improve the chances of finding a feasible dispatch solution by balancing generation and demand.

Here we focus the configuration of the simulation on the QSS group of parameters to better evaluate similarities and differences with respect to the dynamic simulator. For example, a tunable aspect in *dcsimsep* is the *pseudo*-time allowed for generator rampings, that is, discretizing the next QSS timestep where the power flow is calculated by performing a generator output projection before advancing the solver to the next steady-state timestep. By starting with a minimum fixed value, e.g., 60 seconds, of ramping that is allowed before resorting to load shedding to balance the island, we can later reproduce as similar behavior as possible in the dynamic simulator by tuning the machines' inertia to equivalent values.

5.1.4 A Dynamic Model Example

By choosing a dynamic model example, *COSMIC* [4], that is built upon the same code baseline as the QSS example, we try to focus the experiments in the remainder of this chapter on their direct similarities and differences, while minimizing baseline noise coming from possible discrepancies across different families of simulators and implementations on substantially different platforms.

The dynamics of a power system can be described with a set of hybrid differential (**f**) and algebraic (**g**) equations [3, 21], where hybrid refers to the addition of a set of equations (**h**) that represent discrete events (for example, a relay trip). The resulting hybrid differential–algebraic system of equations (DAE) is given by

$$\begin{aligned} \frac{d\mathbf{x}(t)}{dt} &= \mathbf{f}(t, \mathbf{x}(t), \mathbf{y}(t), \mathbf{z}(t)) \\ \mathbf{0} &= \mathbf{g}(t, \mathbf{x}(t), \mathbf{y}(t), \mathbf{z}(t)) \\ \mathbf{0} &> \mathbf{h}(t, \mathbf{x}(t), \mathbf{y}(t), \mathbf{z}(t)), \end{aligned} \tag{5.2}$$

where $\mathbf{x}(t)$ is a vector of continuous state variables linked to the differential equations, $\mathbf{y}(t)$ is a vector of continuous state variables linked to the algebraic equations, and $\mathbf{z}(t)$ is a vector of discrete state variables. There are different options in *COSMIC* to solve the differential portion of the system, for example, Matlab's standard functions *ode15s* and *ode23t* [20], which feature an interface to compute a semi-explicit DAE system with a direct approach. The most challenging part of this approach is the initialization of the integration, in particular, right after discrete events. At these breaking points, *COSMIC* uses a nonlinear solver to calculate where to "reconnect" the upcoming state vectors with the appropriate family of differential

equations that match the current memory of the system. At this point in the time horizon, the options to implement the nonlinear solver in *COSMIC* are similar to the capabilities of *dcsimsep*, and one can customize the function *fsolve* to use external algorithms and settings that work better with the particular power system at hand. To speed up simulation by default, *COSMIC* uses a *trust region* method with *dogleg* implementation that only requires one linear solution per iteration.

A relatively large simulation horizon is computationally expensive for dynamic simulators, and typically, there are developed strategies to speed up without compromising on the mechanisms that are characterized. In the case of the *COSMIC* simulator, a relatively simple approach is to use a variable step size. Here, for the purposes of these experiments and comparative exercise with the QSS simulator, we choose a 10 minute simulation horizon, sufficient to resolve the time constants of the relays. We implement several types of relays:

- Branch temperature relays–overcurrent relays: In order to detect the overload of transmission lines, at each timestep, the simulator updates the temperature portion of the integer state variables ($\mathbf{z}_{temp,i}$) after comparing the current branch temperatures from the differential state vector ($\mathbf{x}(t)$) with the maximum temperature limit for each branch (calculated from the standard IEEE rate line limits) [3].
- Under-voltage and under-frequency relays: After detecting instantaneous off-nominal values for voltage or frequency at each bus (or generator bus), the simulator will apply a relay delay and trip if necessary. In the experiments for this chapter, we use a threshold of 0.87 p.u. for under-voltage and 0.985 p.u. for under-frequency.
- Distance relays: Here we also configure a relatively simple Zone 1 distance relay, tuned at 0.9 p.u.

Another feature implemented in *COSMIC* to accelerate the simulation is the calculation of an equivalent generator set of dynamics for those buses where multiple units exist. We aggregate inertia and capacity as well as tuning the equivalent machine controls. Adapted from [3], the description of the machine dynamics for each generator in *COSMIC* can be summarized by the following elements:

The base equation related to machine dynamics is the standard second-order swing equation, describing rotor speed for a generator connected to Bus i:

$$M\frac{d\overline{\omega_i}}{dt} = P_{m,i} - P_{g,i} - D(\overline{\omega_i} - 1), \tag{5.3}$$

where M is the machine inertia constant, $P_{m,i}$ is the mechanical power input, $P_{g,i}$ is the electrical power output, and D is the machine damping constant.

The rotor angle is given by the equation:

$$\frac{d\delta_i(t)}{dt} = 2\pi f_0(\overline{\omega_i} - 1), \tag{5.4}$$

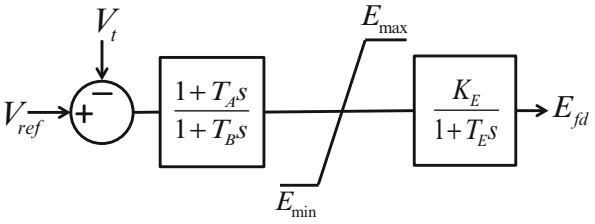

Fig. 5.1 Diagram of the machine exciter model implemented in the *COSMIC* dynamic simulator

and *COSMIC* allows the choice between a standard angle reference or a center-of-inertia reference. This feature is useful to compare and validate across dynamic simulators.

The transient open circuit voltage magnitude is calculated with the differential equation:

$$\frac{d\left|E'_{a,i}(t)\right|}{dt} = -\left|E'_{a,i}\right| \frac{X_{d,i}}{T'_{do,i}X'_{d,i}} + \left(\frac{X_{d,i}}{X'_{d,i}} - 1\right) \frac{|V_i(t)|}{T'_{do,i}} cos(\delta_{m,i}(t)) + \frac{E_{fd,i}}{T'_{do,i}}, \tag{5.5}$$

where $X_{d,i}$ and $X'_{d,i}$ are the direct axis generator synchronous and transient reactances, respectively, $T'_{do,i}$ is the direct axis transient time constant, and $E_{fd,i}$ is the machine exciter output (see Eq. 5.6). The three equations described above describe the basic physical properties of the generator, adding up to a 3rd-order differential equation system. In order to complete the machine model, we add two additional sets of equations describing the machine exciter and the machine governor.

The machine exciter equations define two of the differential variables in $\mathbf{x}(t)$:

$$\begin{array}{rcl} \frac{dE_{fd}}{dt} & = & \frac{1}{T_E}\left(K_E.\text{sigm}\left(\left(1-\frac{T_A}{T_B}\right)E_1 + \frac{T_A}{T_B}(V_{ref}-V_t)\right) - E_{fd}\right) \\ \frac{dE_1}{dt} & = & \frac{1}{T_B}\left(V_{ref} - V_t - E_1\right), \end{array} \tag{5.6}$$

where T_A, T_B, and K_E are exciter time constants, and sigm$(\cdot)$ we write as a differentiable sigmoidal function that acts as a limiter between E_{min} and E_{max}. We implement this function in a way that is similar to *rail limiters* whereby the smooth joints in between linear segments are encoded as differentiable cubic splines. Figure 5.1 illustrates this simplified exciter configuration.

Similarly, we use a similar differentiable rail limiter technique to complete the dynamic model of the generator with a machine governor, describing the mechanical forcing given a deviation in the machine speed:

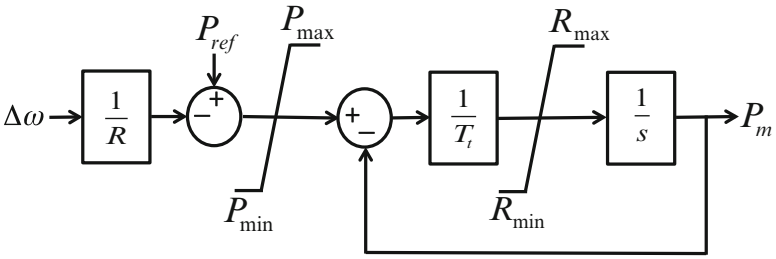

Fig. 5.2 Diagram of the machine governor model implemented in the *COSMIC* dynamic simulator

$$\frac{dP_m}{dt} = \text{sigm}\left(\frac{1}{T_t}(\text{sigm}\left(P_{ref} - \frac{1}{R}\Delta\omega\right)P_2 - P_m)\right), \tag{5.7}$$

where R and T_t are the droop and time constants, respectively. Figure 5.2 describes the interactions among the governor variables and the rail limiters for $P_{\min}$ versus $P_{\max}$ and $R_{\min}$ versus $R_{\max}$.

5.1.5 Benchmark Experiments

For the experiments in this chapter, we focus on the test system IEEE RTS-96 [9], which was also proposed as a good benchmarking network by [10] after some initial adjustments to be initially dispatched as $N-1$ secure. We keep the same modifications for this work. For each cascading failure simulator, we subjected the test grid to $N-2$ and $N-3$ line contingencies. We enumerate all the $N-2$ contingencies (up to a total of 7140 runs) and then simulate an equal number of $N-3$ contingencies, randomly sampled, and resulting on a total of 14,280 runs for all $N-2$ and $N-3$ contingencies.

For the *dcsimsep* simulator, we implement the baseline redispatch mechanisms included in the code package, without additional emergency control activated [6, 13, 19]. In terms of protection, we focus on the mechanisms of separation, load shedding, and line overload relays. At the end of each QSS simulation epoch, we record the initial exogenous events, the dependent endogenous events (including lines tripped), and total load lost.

For the *COSMIC* simulator, we also implement the baseline redispatch mechanisms, in this case an ac algebraic equations resolve that "reconnects" the new algebraic state after a discrete event with the necessary dynamics from the generator machines, exciters, and governors. This is handled as a standard Differential–Algebraic Equation (DAE) solution across discrete events [21], and for consistency, we do not implement additional controls as it is the case in recent applications for this simulator [1]. It is important to note that one of the main relay mechanisms in *COSMIC*, the temperature relay, is an aggregate relay mechanism inspired by the

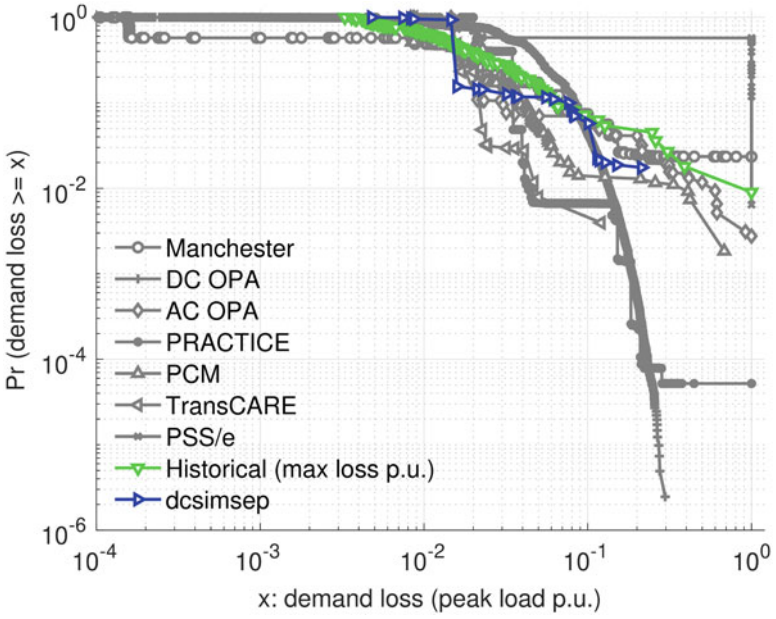

Fig. 5.3 Loss of load distribution for all $N-2$ and equal size set of random $N-3$ contingencies. Comparison between *dcsimsep*, normalized historical data reference, and benchmark QSS simulators from [11]

line overload relay in *dcsimsep*. In order to keep similar rate overload constants for this work, we extended the dynamic simulation horizon in *COSMIC* to 10 minutes, so that we are able to observe those cascades that have an equivalent time horizon in the QSS implementation. Besides the temperature/overload relay, we also implement separation, under-frequency and under-voltage load shedding, distance relays, overcurrent relays, and generator off-nominal frequency trips. At the end of each dynamic simulation epoch, we also record the initial exogenous events, the dependent endogenous events, and total load lost.

5.1.5.1 Size of Blackouts: Load Distributions

The first metric we analyze from the described experiments is the size of the blackouts observed, measured in MW of load not met. We plot these results as a complementary cumulative distribution function (CCDF) that allows us to compare the trends across simulators, and in particular, the areas corresponding to small, medium, or large blackouts, depending on the x-axis region that we focus on. For example, a trace with a heavy tail corresponds with a relatively large probability of observing large blackouts.

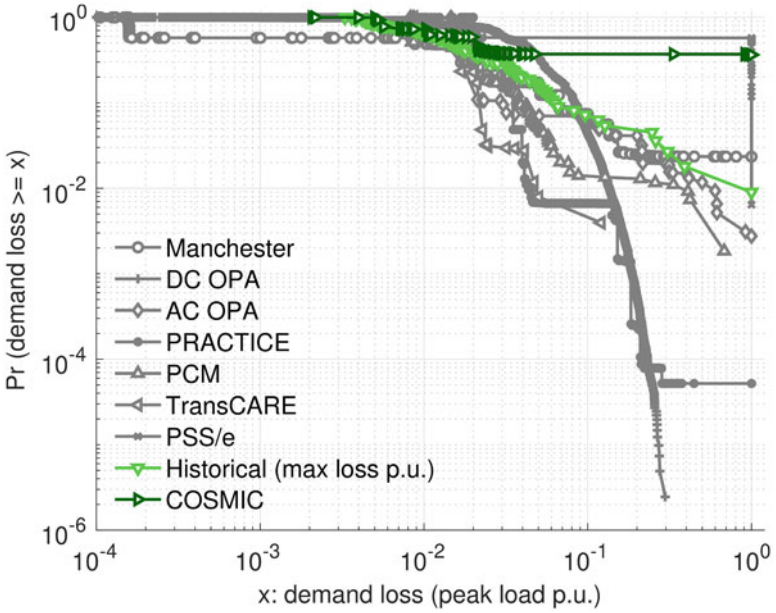

Fig. 5.4 Loss of load distribution for all $N-2$ and equal size set of random $N-3$ contingencies. Comparison between *COSMIC*, normalized historical data reference, and benchmark QSS simulators from [11]

In Fig. 5.3 we can observe the new loss of load distribution obtained with the QSS simulator *dcsimsep* (blue trace) and how it compares with those QSS simulators benchmarked in [11]. Distribution results suggest that *dcsimsep* produces blackouts similar in size with the mid-range group of those in the benchmark set (all grayed out traces for clarity). Also from [11], we highlight (light green trace) the historical data reference, adjusted in per unit to the size of the maximum blackout in the RTS-96. For medium–large blackouts, the *dcsimsep* trace appears similar to the historical reference, a bit under for certain blackout sizes, but overall with a comparable slope.

A recommendation from this analysis is that in order to produce larger blackout sizes with an open-source simulator such as *dcsimsep*, one could adjust the separation mechanisms. Effectively we would be fine-tuning the definition of *when* to consider an island separated as a brownout, continuing to recursively re-balance smaller areas, versus considering that the cascade is finished from the point of view of the original connected components in the network, because we cannot reliably dispatch such small areas. This is relevant as we increase the number of microgrids in our electrical network, as well as other modalities of distributed control, we need to reflect the mechanisms for separation and re-connection accordingly in the simulator, both QSS and dynamic [15].

Analogously, in Fig. 5.4 we can observe the new loss of load distribution obtained with the dynamic simulator *COSMIC* (dark green trace) in the context of the

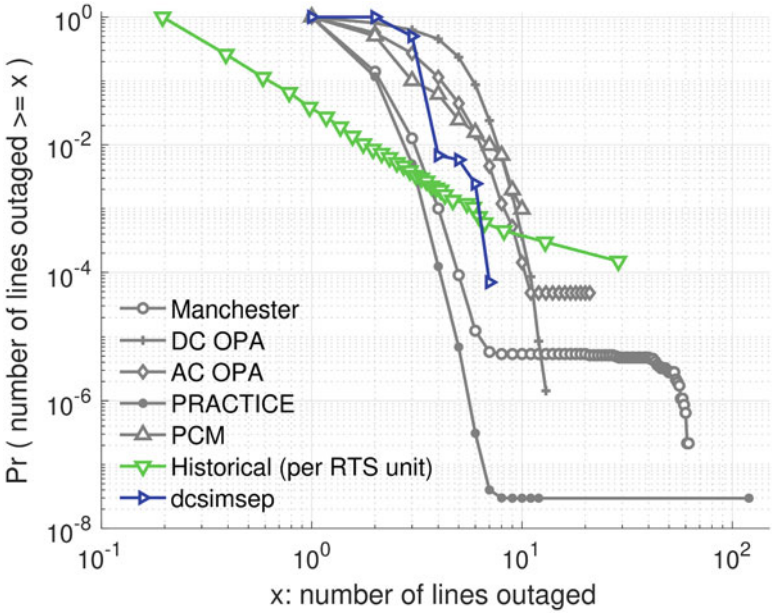

Fig. 5.5 Lines tripped distribution for all $N-2$ and equal size set of random $N-3$ contingencies. Comparison between *dcsimsep*, normalized historical data reference, and benchmark QSS simulators from [11]

datasets from [11]. In this case, small and medium blackout sizes follow fairly well the historical trend and benchmark QSS simulators. For large blackout sizes, the relatively heavier tail captures the behavior of possible dynamic instability for networks that are largely disturbed and tend to produce full outages (although this is not exclusive to dynamic simulators, as the trace corresponding to PSS/e shows, with some higher probabilities for the maximum size. That being said, the trace corresponding to *COSMIC* reflects the appearance of very large blackouts that are not full system collapse, and this certainly merits further exploration of the individual cascades so that it sheds light on the particular mechanism differentiating from the QSS trends in this benchmark ensemble.

5.1.5.2 Line Distributions

The second metric we analyze for this set of experiments is the distribution of transmission lines that were outaged. It is important to note that we include in this section all the lines that were removed from service in the $N-2$ and $N-3$ cascades, either by the initial events or by the subsequent dependent relay trips. In the next section, we will explore the differences between the two subsets (initial or dependent outages) in terms of line criticality by means of frequency of appearance.

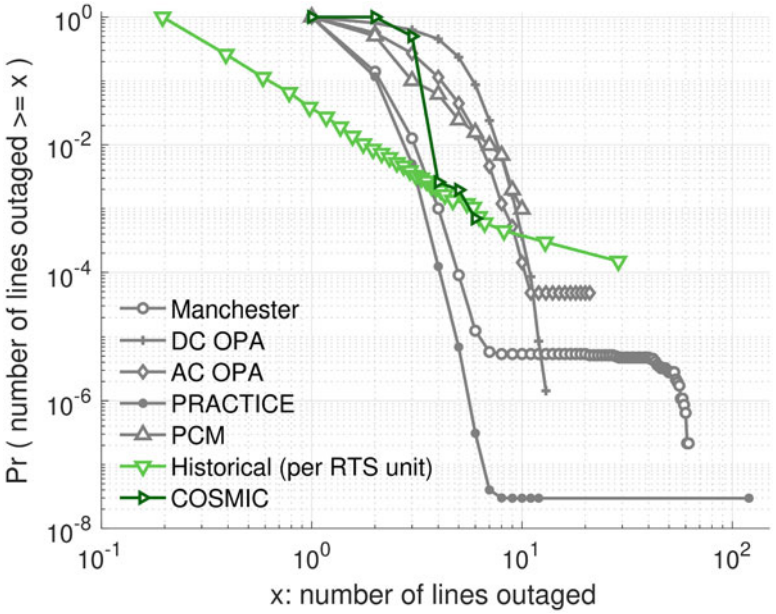

Fig. 5.6 Lines tripped distribution for all $N-2$ and equal size set of random $N-3$ contingencies. Comparison between *COSMIC*, normalized historical data reference, and benchmark QSS simulators from [11]

In Fig. 5.5, we compare the distribution of the number of lines outaged for *dcsimsep* with the historical reference and simulator benchmarks from [11]. It is encouraging that the trace shape for the medium–large size cascades (4,5,6, or 7 lines) approaches the historical trend.

We also note the difference with other simulators that obtain a much larger number of transmission lines tripped. As we discussed earlier with the threshold to consider the system separation as a terminating event or part of the cascade, it would be important also to define what is an upper bound on lines outaged for a given system size where one would expect the cascading simulation to still be meaningful. In this experiment's scale, for a system size like the RTS-96 with 120 lines, it is difficult to interpret how the simulation mechanisms continue in a similar regime after the relays tripped line $100th$ out of 120, for example. It appears that the overall distribution of lines cascaded is most similar between the *dcsimsep* and *PCM* QSS simulators.

For the dynamic simulation comparison, in Fig. 5.6, we see a similar trend for the lines outaged distribution in the *COSMIC* simulator, whereby the medium size cascades matched most closely the historical trend among all the benchmarks.

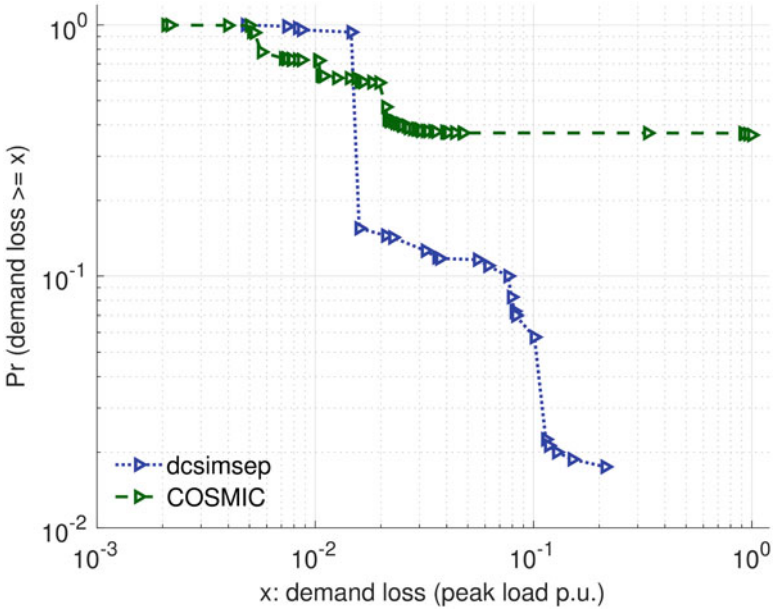

Fig. 5.7 Side-by-side comparison between *dcsimsep* and *COSMIC* simulators for the distribution of demand lost

5.1.5.3 Summary of Statistical Similarities and Differences Between *dcsimsep* and *COSMIC*

Here we compare side by side, according to the previous metrics in this section, our QSS example simulator, *dcsimsep*, and our dynamic example simulator, *COSMIC*. First for distribution of load lost, in Fig 5.7, we see higher similarities for small blackouts; however, for medium and large blackouts, the distributions for demand loss start to diverge. It is worth to note here that as we have discussed so far, we prioritized in this batch of experiments to equalize the overload relays to be able to compare the trajectories of the cascades between both the QSS and dynamic simulators. Another approach for future work could be to maintain as much similarity as possible with load shedding relays as well, although this is best achieved by working in some additional dispatch control, a feature that both example simulators implement.

Figure 5.8 suggests that the similarities between the lines tripped distributions are stronger and follow a very similar pattern for medium-sized cascades. The output in *dcsimsep* produced a few longer cascades, but the probability of those quickly falls.

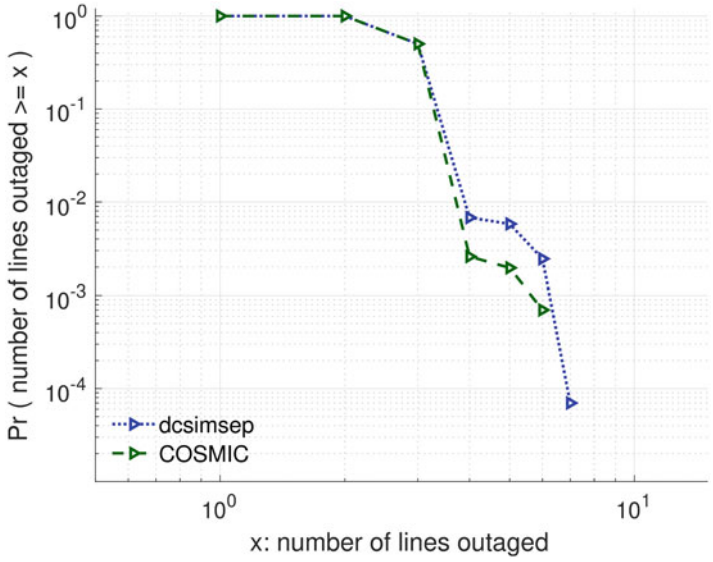

Fig. 5.8 Side-by-side comparison between *dcsimsep* and *COSMIC* simulators for the distribution of lines outaged

5.1.5.4 Cascade Sequence Benchmarks

In this section, we turn to explore the similarities and differences of the cascading sequences for both the QSS and dynamic simulators, with the same set of $N-2$ and $N-3$ experiments on the IEEE RTS-96 network. First, we measure the relative agreement of cascading path, R, among all the simulated initiating events, and then solely grouped by $N-2$ or $N-3$ types. Table 5.1 shows that the agreement between the simulators is substantially higher when analyzing the $N-2$ initiating events, whereas R decreases on the $N-3$ subset. The number of cascades that fall in one type versus the other is approximately a 25%/75% split.

5.1.5.5 Rank of Top 5 Critical Components Involved in Initial Outages

Now we turn to discuss the involvement of common initiating sets of lines in subsequent outages. From the set of $N-2$ and $N-3$ experiments, we count and rank those lines that more frequently appear as initial outage at the beginning of a cascade. In Table 5.2, we compare the results for *dcsimsep* on the left panel with *COSMIC* on the right panel. The five rows of data across both panels represent the Top 5 branches (including those that are tied in one of the five given positions), the line identifier, and the frequency of appearance in the full set of simulation epochs. After highlighting in boldface the line numbers that are common to both simulators, we can observe a very high degree of similarity, whereby 100% of those initial

Table 5.1 Relative agreement of cascading path for *dcsimsep* (m_1) and *COSMIC* (m_2) among all simulated initiating events and the $N-2$, $N-3$ subsets

	$R(m_1, m_2)$	$\|C\|$
$N-2$ and $N-3$	0.2686	103 cascades
$N-2$	0.5641	26 cascades
$N-3$	0.1688	77 cascades

Table 5.2 Rank of Top 5 critical components and their frequency of appearance within initial outages that cause cascades

dcsimsep			*COSMIC*		
Rank	Line number	Frequency	Rank	Line number	Frequency
Top 1	**30**	×18	Top 1	**27**	×8
Top 2	**7**	×15	Top 2	**7**, **30**	×7
Top 3	**27**, **31**	×14	Top 3	**28**, **31**, **69**	×6
Top 4	**26**, **66**, **69**	×12	Top 4	25, **29**, **66**, 119	×5
Top 5	**28**, **29**, **67**	×11	Top 5	**26**, **67**, 101	×4

contingencies that are Top 5 for *dcsimsep* appear on the panel corresponding to the *COSMIC* simulator, with only 3 lines that are not a commonality appearing on the dynamic simulator results.

5.1.5.6 Rank of Top 5 Critical Components Involved in Subsequent Outages

Similarly to the previous subsection, we now discuss the involvement of common subsequent sets dependent lines outages, with respect to both simulators, from the set of $N-2$ and $N-3$ experiments. In Table 5.3, we compare again the results for *dcsimsep* on the left panel with *COSMIC* on the right panel. In this case, after highlighting in boldface the line numbers that are common to both simulators, we also obtain a very high overall similarity on both sets, with an 80% agreement on the lines that appear on the Top 5 critical elements for both *dcsimsep* and *COSMIC*. Only lines 11 and 25 appeared in one or the other simulator but not both. It is important to note that overall, the set of dependent critical outaged lines is also more concentrated in fewer number of lines with higher frequency of appearance in cascading sequences, for both the QSS and the dynamic simulator. This suggests that any mitigation measures that focus on the propagating lines are likely to help reduce the overall risk, independently of whether one uses the QSS or the dynamic simulator version for this test case.

Table 5.3 Rank of Top 5 critical components and their frequency of appearance within initial outages that cause cascades

dcsimsep			*COSMIC*		
Rank	Line number	Frequency	Rank	Line number	Frequency
Top 1	**119**	×58	Top 1	**118**	×26
Top 2	11	×16	Top 2	**119**	×26
Top 3	**30**	×16	Top 3	**30**	×8
Top 4	**41**	×16	Top 4	**41**	×7
Top 5	**118**	×14	Top 5	25	×6

5.1.6 Conclusions and Future Work

In this chapter, we have presented a discussion of similarities and differences between quasi-steady-state (QSS) and dynamic models of cascading outages. We discuss new findings obtained from side-to-side comparison experiments between QSS and dynamic simulators that stem from related branches of open-source codes. We also positioned this analysis with respect to previous results obtained by recent benchmarking studies that included both research-grade and commercial simulator software. For future work, we recommend the concurrent use of multiple simulation fidelities in cascading outage studies, as well as the inclusion, early in the workflow, of real datasets for calibration and validation of the relay mechanisms in the models being considered.

References

1. F. Alanazi, J. Kim, E. Cotilla-Sanchez, Load oscillating attacks of smart grids: vulnerability analysis. IEEE Access **11**, 36538–36549 (2023). ISSN: 2169-3536. https://doi.org/10.1109/ACCESS.2023.3266249. https://ieeexplore.ieee.org/document/10098782/ (visited on 08/29/2023)
2. J. Bialek et al., Benchmarking and validation of cascading failure analysis tools. IEEE Trans. Power Syst. **31**(6), 4887–4900 (2016). ISSN: 08858950. https://doi.org/10.1109/TPWRS.2016.2518660
3. E. Cotilla-Sanchez, Big data and energy systems: efficient computational methods for the dynamic analysis of electric power infrastructure. PhD thesis. University of Vermont, 2012
4. E. Cotilla-Sanchez, *ecotillasanchez/cosmic*, Aug. 2023. https://github.com/ecotillasanchez/cosmic (visited on 08/30/2023)
5. Y. Dai et al., Risk assessment and mitigation of cascading failures using critical line sensitivities. IEEE Trans. Power Syst., 1–12 (2023). ISSN: 0885-8950, 1558-0679. https://doi.org/10.1109/TPWRS.2023.3305093. https://ieeexplore.ieee.org/document/10219000/ (visited on 08/27/2023)
6. M.J. Eppstein, P.D.H. Hines, A "random chemistry" algorithm for identifying collections of multiple contingencies that initiate cascading failure. IEEE Trans. Power Syst. **27**(3), 1698–1705 (2012). ISBN: 9781479913039. ISSN: 08858950. https://doi.org/10.1109/TPWRS.2012.2183624

7. R. Fitzmaurice, E. Cotilla-Sanchez, P. Hines, Evaluating the impact of modeling assumptions for cascading failure simulation, in *IEEE Power and Energy Society General Meeting*. ISSN: 19449925.2012. ISBN: 978-1-4673-2727-5. https://doi.org/10.1109/PESGM.2012.6345378
8. A.J. Flueck et al., Dynamics and protection in cascading outages, in *2020 IEEE Power & Energy Society General Meeting (PESGM)* (IEEE, Montreal, QC, Canada, Aug. 2020), pp. 1–5 ISBN: 978-1-72815-508-1. https://doi.org/10.1109/PESGM41954.2020.9281823. https://ieeexplore.ieee.org/document/9281823/ (visited on 08/30/2023)
9. C. Grigg, P. Wong, The IEEE reliability test system—1996 a report prepared by the reliability test system task force of the application of probability methods subcommittee. IEEE Trans. Power Syst. **14**(3), 1010–1020 (1999). ISBN: 0885-8950. ISSN: 08858950. https://doi.org/10.1109/59.780914
10. P. Henneaux et al., A two-level probabilistic risk assessment of cascading outages. IEEE Trans. Power Syst. **31**(3), 2393–2403 (2016)
11. P. Henneaux et al., Benchmarking quasi-steady state cascading outage analysis methodologies, *2018 IEEE International Conference on Probabilistic Methods Applied to Power Systems (PMAPS)* (IEEE, Boise, ID, June 2018), pp. 1–6. ISBN: 978-1-5386-3596-4. https://doi.org/10.1109/PMAPS.2018.8440212. https://ieeexplore.ieee.org/document/8440212/ (visited on 08/04/2023)
12. P. Hines, *DCSIMSEP*, June 2023. https://github.com/phines/dcsimsep (visited on 08/30/2023)
13. P. Hines, E. Cotilla-Sanchez, S. Blumsack, Do topological models provide good information about electricity infrastructure vulnerability? Chaos **20**(3) (2010). arXiv:1002.2268. ISBN: 1054-1500. ISSN: 10541500. https://doi.org/10.1063/1.3489887
14. W. Ju, K. Sun, R. Yao, Simulation of cascading outages using a power flow model considering frequency. IEEE Access (2018). IEEE, p. 1. https://doi.org/10.1109/ACCESS.2018.2851022
15. C. Lassetter, E. Cotilla-Sanchez, J. Kim, A learning scheme for microgrid reconnection. IEEE Trans. Power Syst. **33**(1), 691–700 (2018). ISSN: 0885-8950, 1558-0679. https://doi.org/10.1109/TPWRS.2017.2709741. http://ieeexplore.ieee.org/document/7935511/ (visited on 05/16/2020)
16. L. Niu et al., *A Hybrid Submodular Optimization Approach to Controlled Islanding with Post-Disturbance Stability Guarantees*. arXiv:2302.10308 [cs, eess, math], Feb. 2023. http://arxiv.org/abs/2302.10308 (visited on 02/27/2023)
17. M. Papic, S. Ekisheva, E. Cotilla-Sanchez, A risk-based approach to assess the operational resilience of transmission grids. Appl. Sci. **10**(14), 4761 (2020). ISSN: 2076-3417. https://doi.org/10.3390/app10144761. https://www.mdpi.com/2076-3417/10/14/4761 (visited on 07/11/2020)
18. M. Papic et al., Multiple outage challenges to transmission grid resilience, in *2019 IEEE Power & Energy Society General Meeting* (*PESGM*) (IEEE, Atlanta, GA, USA, Aug. 2019), pp. 1–5. ISBN: 978-1-72811-981-6. https://doi.org/10.1109/PESGM40551.2019.8973606. https://ieeexplore.ieee.org/document/8973606/ (visited on 02/03/2020)
19. P. Rezaei, P.D.H. Hines, M.J. Eppstein, Estimating cascading failure risk with random chemistry. IEEE Trans. Power Syst. **30**(5), 2726–2735 (2015). arXiv:1405.4213. ISBN:9781467380409. ISSN: 08858950. https://doi.org/10.1109/TPWRS.2014.2361735
20. L.F. Shampine, M.W. Reichelt, J.a. Kierzenka, Solving Index-1 DAEs in MATLAB and simulink. SIAM Rev. **41**(3), 538–552 (1999). ISSN: 0036-1445. https://doi.org/10.1137/S003614459933425X
21. J. Song et al., Dynamic modeling of cascading failure in power systems. IEEE Trans. Power Syst. **31**(3), 2085–2095 (2016). arXiv:1411.3990. https://doi.org/10.1109/TPWRS.2015.2439237
22. R. Yao et al., A multi-timescale quasi-dynamic model for simulation of cascading outages. IEEE Trans. Power Syst. **31**(4), 3189–3201 (2016). ISSN: 08858950. https://doi.org/10.1109/TPWRS.2015.2466116